deformation. This permitted us to discuss the following: (i) The coupling coefficient C_E of Eq. (24). This is the Van Vleck's[16,15] coefficient V. (ii) We pointed out that there was a pair of *trigonal* deformations Q_ϵ and Q_θ in Fig. 6, which seem to behave like the corresponding cubic pair,[2,16] and therefore a selection of cubic coordinates for analysis is an unnecessary simplification. (iii) Besides the familiar energies of the excited levels Δ_O, Δ_C, and Δ_S, it was possible to estimate the energy of separation Δ_θ of the ground $2E_g$ doublet and also the Jahn–Teller stabilization energy. (iv) On this basis one could also account for some other features such as the appearance of A_{xz}.

*Supported by the National Research Council of Canada.

[1]R. G. Wilson, F. Holuj, and N. E. Hedgecock, Phys. Rev. B **1**, 3609 (1970).
[2]F. S. Ham, General Electric Technical Inf. Ser. Report No. 68-L-248, 1968 (unpublished).
[3]M. D. Sturge, in *Solid State Physics,* edited by F. Seitz, D. Turnbull, and H. Ehrenreich (Academic, New York, 1967), Vol. 20.
[4]F. Holuj, Can. J. Phys. **46**, 287 (1968).
[5]J. S. Griffith, *Transition Metal Ions* (Cambridge U. P., Cambridge, England, 1961).
[6]F. M. O. Michel-Calendini and M. R. Kibler, Theor. Chim. Acta **10**, 367 (1968).
[7]A. Abragam and B. Bleaney, *Electron Paramagnetic Resonance of Transition Elements* (Oxford, U. P., London, 1970).
[8]J. Owen and J. H. M. Thornley, Rep. Prog. Phys. **29**, 675 (1966).
[9]B. R. McGarvey, J. Phys. Chem. **71**, 51 (1967).
[10]C. Basu and U. S. Ghosh, J. Phys. Chem. Solids **32**, 2259 (1971).
[11]B. Bleaney, K. D. Bowers, and D. J. E. Ingram, Proc. R. Soc. A **228**, 147 (1955).
[12]B. Bleaney, K. D. Bowers, and R. S. Trenam, Proc. R. Soc. A **228**, 157 (1955).
[13]B. Bleaney, K. D. Bowers, and M. H. L. Pryce, Proc. R. Soc. A **228**, 166 (1955).
[14]M. C. M. O'Brien, Proc. R. Soc. A **281**, 323 (1964).
[15]U. Opik and M. H. L. Pryce, Proc. R. Soc. A **238**, 425 (1957).
[16]J. H. van Vleck, J. Chem. Phys. **1**, 72 (1939).

PHYSICAL REVIEW B VOLUME 7, NUMBER 9 1 MAY 1973

Spin-Lattice Coupling Coefficients of a $3d^5$ Ion in Trigonal Symmetry: Study of Mn^{++} in Zinc Sulfide

C. Blanchard
Laboratoire d'Electronique, Université de Provence, Saint-Jérôme, 13013 Marseille, France

R. Parrot and D. Boulanger
Laboratoire de Luminescence II, Université de Paris VI, 4, Place Jussieu-75230 Paris Cedex 05, France

(Received 25 July 1972)

The spin-lattice coupling coefficients of Mn^{++} in C_{3v} symmetry have been measured by a uniaxial-stress method. The two axial sites studied experimentally correspond to an axial-field parameter $D = -130.9 \times 10^{-4}$ cm^{-1}. Since the structure of these sites is not yet known, we performed theoretical calculations of the spin-lattice coupling coefficients for all the different sites which can exist in ZnS. The coefficients were calculated in an ionic model, following a perturbation method proposed by Blume and Orbach and generalized to any pressure-induced distortion. It appears clearly that the components of rank four of the internal crystal field give the preponderant contribution of the spin-lattice coupling coefficients, the influence of the components of rank two being two orders of magnitude smaller. The major contribution to the spin-lattice coupling coefficients C_{ij} is given by the pressure-induced even fields. We show that the equivalent even fields arising from the composition of the internal crystal fields of odd parity with the pressure-induced crystal fields of odd parity contribute significantly to the values of the C_{ij}'s. Several other mechanisms such as spin-spin mechanism and higher-order effects have also been considered. We have shown that the C_{ij}'s would be roughly identical for the different axial sites existing in our samples.

I. INTRODUCTION

If the $3d^5$ ions in cubic and trigonal symmetry have been extensively studied in EPR experimentally as well as theoretically; there have been fewer studies made on the variations of the parameters of the spin Hamiltonian and pressure-induced terms of this Hamiltonian under the action of uniaxial stresses. In fact, since the determination of the spin-lattice coupling coefficients (SLCC) of Mn^{++} and Fe^{3+} in MgO by Feher, [1] the majority of experiments of this type have been carried out on ions other than $3d^5$. [2,3]

A theoretical study of the zero-field splitting of

^6S-state ions was made by Sharma, Das, and Orbach.[4-6] They studied in a very detailed manner the influence of the spin-spin and spin-orbit interactions in an ionic and a covalent model. In the case of MnF_2,[4] Mn^{++} in ZnF_2,[4,5] and Mn^{++} in distorted MgO host lattice[6] they showed the importance of these interactions in the determination of the effect of axial and rhombic deformations on the zero-field splitting. They also showed that for Mn^{++} in these compounds, covalency does not give a very important contribution. However, for other $3d^5$ ions and for other environments, covalent effects may be predominant. Recently, Han, Rettig, and Das[7] have found in hemin chloride a very strong enhancement of the spin-orbit and spin-spin interactions by covalency.

More specifically, Sharma[8] showed that the spin-spin interaction and the spin-orbit interaction treated in the ionic case by a perturbation procedure proposed by Blume and Orbach[9] give correct results for Mn^{++} in $CdCl_2$. Our interpretation of the SLCC's of Mn^{++} in ZnS is based primarily on this perturbation procedure.

In Sec. II, the pressure-induced terms appearing in the spin Hamiltonian are given for a C_{3v} symmetry. General relations are derived which permit us to relate the shifts of the absorption lines with the SLCC's for any relative orientation of the magnetic field and stresses with respect to the crystallographic axes.

In Sec. III we give the results of the experiments on Mn^{++} in ZnS. We studied only the SLCC's of the axial centers corresponding to an axial-field parameter $D = -130.9\times10^{-4}$ cm^{-1}.[10] Our samples also contained two other axial centers with $D = +36.1\times10^{-4}$ cm^{-1}[11] and two cubic centers.[10]

The theory of the SLCC's in the case of a C_{3v} symmetry is presented in Sec. IV. The perturbation procedure proposed by Blume and Orbach[9] is generalized in order to express the new terms appearing in the spin Hamiltonian in terms of the matrix elements of the spin-orbit interaction (relating the fundamental state with the optical states $^4T_1$) and in terms of the matrix elements of the internal-pressure-induced crystal field between the relevant optical levels. Among all other mechanisms which can contribute to the SLCC's, we studied particularly the influence of the pressure-induced crystal field of odd parity.

The comparison of the experimental results with theory is done in Sec. V, the structure of the axial centers studied experimentally not being well defined, we considered the simplest stacking fault to explain the presence of all the different sites existing in our sample. We then performed theoretical calculations for all the axial sites in ZnS (including the case of Mn^{++} in wurtzite). We show that in the Blume and Orbach scheme, the crystal fields of rank four give the most important contribution to the SLCC's and that higher-order effects such as the Watanabe mechanism and Das–Orbach–Sharma mechanism[4] are negligible. We also show that the spin-spin interaction and the odd crystal fields give non-negligible although non-preponderant contributions.

II. SPIN HAMILTONIAN

For the experimental determination of the SLCC's it is very convenient to express the shifts of the absorption lines in terms of the stress tensor, while the strain tensor will be more adapted to the theoretical calculations. We will write the new term $\Delta\mathcal{H}$ of the spin Hamiltonian in the following manner:

$$\Delta\mathcal{H}=\sum_{i,j} S_i\,\delta D_{ij} S_j+\sum_{i,j} S_i\,\delta g_{ij} H_j + (\text{higher-order terms in } S \text{ and } H).$$

In our case, we consider only the new terms quadratic in S and linear with respect to the stresses (or to the strains). The tensor δD_{ij} is real, since $\Delta\mathcal{H}$ is invariant under time-reversal symmetry and is symmetric, since the antisymmetric part of $\Delta\mathcal{H}$ gives terms linear in S. We can relate the symmetric tensor δD_{ij} to the symmetric stress tensor X_{ij} by a rank-four tensor C_{ijkl}; this last tensor being symmetric only with respect to i and j, and k and l, but not for a permutation of ij and kl, as is the elasticity tensor.[12] Thus, the tensor $\underline{C}$ is analogous to the photoelastic tensor and to the pressure-induced electrical-conductivity tensor.[13,14] This tensor possesses eight independent coefficients for a symmetry C_{3v}. Since a shift common to all levels cannot be measured by EPR techniques, the notations will be simplified by arbitrarily taking

$$\sum_i \delta D_{ii} = 0, \quad i = 1, 2, 3.$$

Two independent relations can be derived from this identity, giving

$$C_{33} = -2C_{13}, \quad C_{31} = -(C_{11} + C_{12}).$$

Thus, six independent coefficients can be measured. The $\underline{C}$ tensor will be determined in an axis system (x, y, z) such that $\vec{x}$ is in a mirror plane and $\vec{z}$ is along the c axis. $\Delta\mathcal{H}_{\text{stress}}$ is given by the contracted multiplication

$$\Delta\mathcal{H}_{\text{stress}} = (\underline{C}\times\underline{X}\times\underline{S})_{\text{contracted}},$$

where $\underline{X}$ is the stress tensor. Explicitly, in the chosen axis system, we get

$$\Delta\mathcal{H}_{\text{stress}} = (C_{11}X_{11}+C_{12}X_{22}+2C_{15}X_{13}+C_{13}X_{33})S_1^2 + (C_{12}X_{11}+C_{11}X_{22}+C_{13}X_{33}-2C_{15}X_{13})S_2^2$$
$$+ [C_{31}(X_{11}+X_{22})+C_{33}X_{33}]S_3^2 + (2C_{44}X_{23}-2C_{51}X_{12})(S_2S_3+S_3S_2)$$
$$+ [C_{51}(X_{11}-X_{22})+2C_{44}X_{13}](S_1S_3+S_3S_1) + [-2C_{15}X_{23}+(C_{11}-C_{12})X_{12}](S_1S_2+S_2S_1),$$

where indices 1, 2, 3 correspond, respectively, to axes $\vec{x}$, $\vec{y}$, $\vec{z}$. It must be noted that the two indices of the C's are defined by the correspondence $1\rightarrow 11$, $2\rightarrow 22$, $3\rightarrow 33$, $4\rightarrow 23$, $5\rightarrow 13$, $6\rightarrow 12$; no factor of 2 being introduced in this notation.

In the theoretical calculations of the SLCC's it is more convenient to evaluate the coefficients of the $\underline{G}$ tensor defined by

$$\Delta\mathcal{H}_{\text{strain}} = (\underline{G}\times\underline{\epsilon}\times\underline{S})_{\text{contracted}},$$

where $\underline{\epsilon}$ is the strain tensor. In that case, in the same axis system as used previously, we get $G_{46} = 2G_{51}$ and $G_{66}=\frac{1}{2}(G_{11}-G_{12})$ instead of $C_{46}=C_{51}$ and $C_{66}=C_{11}-C_{12}$, for the $\underline{C}$ tensor. The tensors $\underline{G}$ and $\underline{C}$ are related by the elasticity tensor

$$G_{ijkl}s_{klrs} = C_{ijrs},$$

the contraction being done evidently on the indices k and l. The theoretical determination of the G_{ijkl}'s necessitates the knowledge of the spin Hamiltonian in the same axis system as that used for the determination of the wave functions intervening in the theoretical calculations.

For the experimental determination of the C_{ijkl}, it is necessary to know the relation between the SLCC's and the shifts of the EPR lines in any axis system. We will give below the most general relations permitting the proper choice of the direction of the applied pressure and of the magnetic field with respect to the crystallographic axes. The Hamiltonian can be expressed simply in terms of the tensor operators $O^{(k)}$ defined by Smith and Thornley.[15] If we use the identity

$$\sum_i D_{ii}S_i^2 = \tfrac{2}{3}[D_{33}-\tfrac{1}{2}(D_{11}+D_{22})][S_3^2-\tfrac{1}{2}(S_1^2+S_2^2)] + \tfrac{1}{2}(D_{11}-D_{22})(S_1^2-S_2^2) + \tfrac{1}{3}\sum_{ij} D_{ii}S_j^2,$$

with the additional convention $\sum_i D_{ii}=0$, we get

$$\mathcal{H}_{\text{stress}} = D_{33}O_0^{(2)} + \left(\frac{1}{\sqrt{6}}(D_{11}-D_{22}) - \frac{i\sqrt{2}}{\sqrt{3}}D_{12}\right)O_2^{(2)}$$
$$+ \left(\frac{1}{\sqrt{6}}(D_{11}-D_{12}) + \frac{i\sqrt{2}}{\sqrt{3}}D_{12}\right)O_{-2}^{(2)} - \frac{\sqrt{2}}{\sqrt{3}}(D_{13}-iD_{23})O_1^{(2)} + \frac{\sqrt{2}}{\sqrt{3}}(D_{13}+iD_{23})O_{-1}^{(2)}.$$

It is convenient to rotate the tensor $\underline{D}$, the new terms of the rotated tensor $\underline{D}'$ being expressed in a compact form by

$$D'_{mn} = [\tfrac{1}{2}(C_{11}+C_{12})(X_{11}+X_{22})+C_{13}X_{33}](\delta_{mn}-3a_{m3}a_{n3})$$
$$+ \tfrac{1}{2}(C_{11}-C_{12})[(a_{m1}a_{n1}-a_{m2}a_{n2})(X_{11}-X_{22}) + 2(a_{m1}a_{n2}+a_{m2}a_{n1})X_{12}]$$
$$+ 2C_{44}[(a_{m2}a_{n3}+a_{m3}a_{n2})X_{23}+(a_{m1}a_{n3}+a_{m3}a_{n1})X_{13}] + 2C_{15}[(a_{m1}a_{n1}-a_{m2}a_{n2})X_{13}-(a_{m1}a_{n2}+a_{m2}a_{n1})X_{23}]$$
$$+ 2C_{51}[-(a_{m2}a_{n3}+a_{m3}a_{n2})X_{12}+\tfrac{1}{2}(a_{m1}a_{n3}+a_{m3}a_{n1})(X_{11}-X_{22})],$$

the a_{mn}'s are the elements of the matrix of rotation.

If we consider the terms in the spin Hamiltonian proportional to the axial-field parameter D and pressure, the second-order correction of the energy levels is connected only to the nondiagonal terms of the spin Hamiltonian corresponding to $\Delta M_S=\pm 1$ and $\Delta M_S=\pm 2$, that is, only the tensor operators $O_{\pm 1}^{(2)}$ and $O_{\pm 2}^{(2)}$ will intervene in our expressions. In this section we have neglected the terms proportional to the fine-structure constant a and to pressure, since these terms are negligible in our experiments. The perturbation procedure used here will be applicable to magnetic ions for which D and a are small compared to $g\mu_B H$, H being the static magnetic field at the resonance. We will give here the general expression for the shifts of the energy levels for any orientation of the pressure in the case of a C_{3v} symmetry. For a transition $M_S\rightarrow M_S-1$, the terms linear in P and bilinear in D and P give the following shifts:

$$g\mu_B\Delta H = AD'_{33} + BD'_{13}a_{13}a_{33} + C(D'_{11}-D'_{22})a_{13}^2,$$

with

$$A = \tfrac{3}{2}(1-M_S),$$

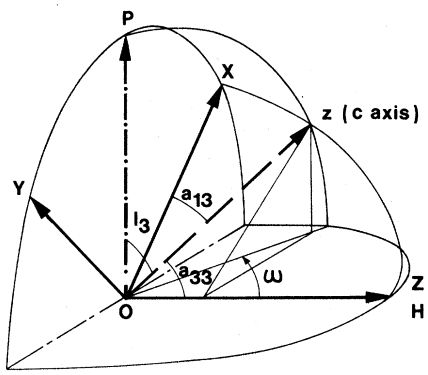

FIG. 1. Axis system used in the experiments. Applied pressure is located in the (x, y, z) axis system (only $\vec{z}$ is represented); $\vec{z}$ corresponds to the c axis. The magnetic field $\vec{H}$ and the c axis define an axis system (X, Y, Z); $\vec{H}$ is along the $\vec{Z}$ axis and the c axis is in the plane ZOX. The a_{ij}'s defined in Sec. II are the elements of the matrix of rotation associated to these two axes systems. ω is the measured angle, that is, the angle between $\vec{H}$ and the projection of the c axis on a plane perpendicular to the applied pressure $\vec{P}$.

$$B = \frac{4D}{3g\mu_B H}\left[3S(S+1) - \tfrac{9}{4}(8M_S^2 - 8M_S + 3)\right],$$

$$C = \frac{D}{6g\mu_B H}\left[-3S(S+1) + \tfrac{9}{4}(4M_S^2 - 4M_S + 2)\right],$$

S being the spin. Expanding the D'_{ij}'s in terms of the C_{ij}'s, we get

$$g\mu_B \Delta H = \xi_1\left(A + B\frac{3a_{13}^2 a_{33}^2}{3a_{33}^2 - 1} + C\frac{3a_{13}^4}{a_{33}^2 - 1}\right) + (\xi_2 + \xi_4)[A - Ba_{33}^2 + C(1 + a_{33}^2)] + (\xi_3 + \xi_5)[A + \tfrac{1}{2}B(a_{13}^2 - a_{33}^2) - Ca_{13}^2],$$

with

$$\xi_1 = [\tfrac{1}{2}(C_{11} + C_{12})(X_{11} + X_{22}) + C_{13}X_{33}](1 - 3a_{33}^2),$$

$$\xi_2 = \tfrac{1}{2}(C_{11} - C_{12})[(a_{31}^2 - a_{32}^2)(X_{11} - X_{22}) + 4X_{12}a_{31}a_{32}],$$

$$\xi_3 = 4C_{44}(a_{32}X_{23} + a_{31}X_{13})a_{33},$$

$$\xi_4 = 2C_{15}[X_{13}(a_{31}^2 - a_{32}^2) - 2X_{23}a_{31}a_{32}],$$

$$\xi_5 = 2C_{51}[-2X_{12}a_{32} + (X_{11} - X_{22})a_{31}]a_{33}.$$

The contribution of the terms bilinear in a and P can be treated in an identical manner. Since they are negligible in our experiments, we will not give the corresponding general relations.

Of course, the angles intervening in the formulas given above must be carefully evaluated in order to permit the determination of the signs of the C_{ij}'s.

III. EXPERIMENTS

The experimental apparatus allows us to apply a static force up to 150 N on the samples in the temperature range 77–300 °K. Slits in the wall of the cavity permit an irradiation of the sample. The cooling is made by a gaseous flow of cold nitrogen. The pressure is applied with a quartz piston, sliding in a quartz tube. Teflon rings avoid the breakdown of the quartz tube inserted in the cavity and subjected to relatively high pressures. Two holes in the tube permit a fast cooling of the sample, if it is necessary.

Many preliminary experiments were made with samples of different sizes and with various cushions between the sample and the piston. For the applied pressure used in our experiments, the best results are obtained with cushions in Teflon and compressed cardboard. Even for very small samples, with dimensions of the order of $1\times1.5\times2$ mm, we can avoid the broadening of the absorption lines due to nonuniaxial stresses in the sample.

Experiments were made on Mn^{++} in ZnS at room temperature. The classical spin Hamiltonian was determined by Schneider *et al.*[10] In the axis system defined in Sec. II, the spin Hamiltonian of the two axial centers studied is

$$\mathcal{H} = g\mu_B \vec{H}\cdot\vec{S} + \tfrac{2}{3}DO_0^{(2)} - \tfrac{2}{45}(a - F)O_0^{(4)} \pm \tfrac{2}{45}(\sqrt{10}/\sqrt{7})\,a(O_3^{(4)} - O_{-3}^{(4)}) + A\vec{I}\cdot\vec{S},$$

with $g_\parallel = 2.0018$, $a = +7.35\times10^{-4}$ cm^{-1}, $D = -130.9\times10^{-4}$ cm^{-1}, $a - F = +7.68\times10^{-4}$ cm^{-1}, and $A = -64.9\times10^{-4}$ cm^{-1}.

The choice of the cuts of the samples was determined from the general relations given in Sec. II. In our case, the magnetic field was perpendicular to the applied pressure $\vec{P}$. The angle ω between the magnetic field $\vec{H}$ and the projection of the c axis on a plane perpendicular to the applied pressure is very convenient because it can be determined experimentally by the position of the absorption lines when $\vec{P} = 0$, the separation of the hexagonal lines being extremum for $\omega = 0$ and $\omega = \pm\frac{1}{2}\pi$. The elements a_{ij} of the matrix of rotation defined in Sec. II can be expressed in terms of ω and in terms of the cosines l_1, l_2, l_3 of the angles between $\vec{P}$ and the crystallographic axes (see Fig. 1),

$$a_{31} = (-l_1 l_3\cos\omega - l_2\sin\omega)(l_1^2 + l_2^2)^{-1/2},$$

$$a_{32} = (-l_2 l_3\cos\omega + l_1\sin\omega)(l_1^2 + l_2^2)^{-1/2},$$

$$a_{33} = (l_1^2 + l_2^2)^{+1/2}\cos\omega,$$

with the additional relation giving the sign of ω,

$$a_{31}l_2 - a_{32}l_1 = -(l_1^2 + l_2^2)^{-1/2}\sin\omega.$$

All other a_{ij}'s can be expressed in terms of the coefficients a_{31}, a_{32}, a_{33}.

For P parallel to the c axis, the shifts are related to C_{13}. In that case, $l_3 = 1$, $a_{33} = 0$, $a_{13}^2 = 1$, $X_{33} = P$, and the other X_{ij}'s are zero. From ξ_1

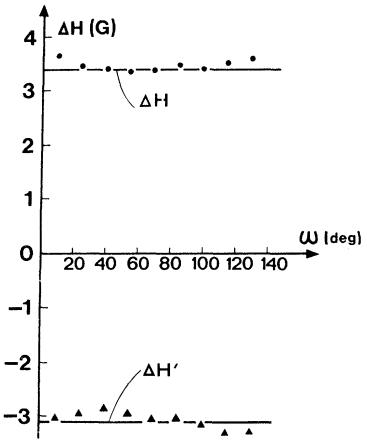

FIG. 2. Angular variations of the stress effect on the hexagonal lines $M_S(+\frac{5}{2} \longleftrightarrow +\frac{3}{2})$ and $M_S(-\frac{3}{2} \longleftrightarrow -\frac{5}{2})$ of Mn^{++} in ZnS. All measurements were made at room temperature. Pressure was applied along the c axis ($P = 2.8\times 10^8$ dyn/cm^2), the magnetic field was rotated in a plane perpendicular to the c axis. The dimensions of the sample were $0.88\times 4.00\times 5.00$ mm, the cross-sectional area perpendicular to the c axis was $(0.88\pm 0.01)(4.00\pm 0.01)$ mm^2.

$= C_{13}P$, $\xi_i = 0$ for $i \neq 1$, we get

$$g\mu_B \Delta H = C_{13}P(A - 3C).$$

The experimental curves are given in Fig. 2. It is convenient to deduce C_{13} from the difference $\Delta H - \Delta H'$, ΔH and $\Delta H'$ being, respectively, the displacements of the lines corresponding to $M_S(-\frac{3}{2} \longleftrightarrow -\frac{5}{2})$ and $M_S(+\frac{5}{2} \longleftrightarrow +\frac{3}{2})$ (for $\vec{H} \perp \vec{c}$, the two axial sites give superimposed absorption lines). With this procedure, the systematic error due to a slight variation of the resonance frequency of the cavity is eliminated; the experimental value of C_{13} is

$$C_{13} = -1.8\times 10^{-13} \text{ cm/dyn}.$$

It must be pointed out that the displacements of the lines are almost constant (Fig. 2), the deviations being due to a slight misorientation of $\vec{H}$ with respect to P. The terms linear in a and P are negligible in this experiment, the contribution due to these terms being less than $\frac{4}{100}$th of the contribution of the terms in DP.

For $\vec{P}$ perpendicular to the c axis and for any orientation of $\vec{P}$ with respect to a mirror plane, we can measure C_{11}, C_{12}, and C_{51}. In that case, $l_3 = 0$, $X_{33} = X_{23} = X_{32} = X_{13} = X_{31} = 0$, and $X_{11} + X_{22} = P$, thus, $\xi_3 = \xi_4 = 0$ and

$$\xi_1 = \tfrac{1}{2}P(C_{11} + C_{12})(1 - 3\cos^2\omega),$$

$$\xi_2 = -\tfrac{1}{2}P(C_{11} - C_{12})\sin^2\omega,$$

$$\xi_5 = \tfrac{1}{2}P C_{51}(4l_2^2 - 3)l_2 \sin\omega\cos\omega .$$

For $l_2 = 1$, the shifts of the absorption lines are

$$g\mu_B\Delta H = \tfrac{1}{2}P(C_{11} + C_{12})[(1 - 3\cos^2\omega)A - (3\sin^2\omega\cos^2\omega)B - 3C\sin^4\omega]$$
$$- \tfrac{1}{2}P(C_{11} - C_{12})\sin^2\omega[A - B\cos^2\omega + C(1 + \cos^2\omega)] \pm \tfrac{1}{2}P C_{51}\sin\omega\cos\omega[A + \tfrac{1}{2}B(\sin^2\omega - \cos^2\omega) - C\sin^2\omega] .$$

The signs + and − correspond to the two axial sites. Figure 3 shows the displacements ΔH_1 and ΔH_2 for the two sites and for the lines $M_S(\frac{5}{2} \longleftrightarrow \frac{3}{2})$ [$\Delta H_1'$ and $\Delta H_2'$ correspond to the lines $M_S(-\frac{3}{2} \longleftrightarrow -\frac{5}{2})$]. The value of $C_{11} + C_{12}$ is deduced from the value of $\frac{1}{2}(\Delta H_1 + \Delta H_2) - \frac{1}{2}(\Delta H_1' + \Delta H_2')$ for $\omega = 0$ (see Fig. 4),

$$C_{11} + C_{12} = 1.84\times 10^{-13} \text{ cm/dyn};$$

for $\omega = \frac{1}{2}\pi$ we get

$$C_{12} \sim -6\times 10^{-15} \text{ cm/dyn},$$

thus

$$C_{11} = 1.9\times 10^{-13} \text{ cm/dyn}.$$

The difference $(\Delta H_1 - \Delta H_2) - (\Delta H_1' - \Delta H_2')$ reported in Fig. 4 is related to C_{51}. By taking this difference, we eliminate the spurious shift of the resonance frequency and we eliminate the first-order contribution of C_{11} and C_{12}. The second-order contribution of C_{12} is negligible with respect to the second-order contribution of C_{11}, which is also negligible, being less than 2×10^{-3} G for any point in Fig. 4. The measured value of C_{51} is

$$|C_{51}| = 0.97\times 10^{-13} \text{ cm/dyn}.$$

The remaining coefficients C_{44} and C_{15} are measured by applying a pressure in a mirror plane at 54° 44′ of the c axis. In this case $l_1 = -\sqrt{\frac{2}{3}}$, $l_2 = 0$, and $l_3 = +1/\sqrt{3}$; $X_{33} = X_{23} = X_{32} = X_{12} = X_{21} = 0$, $X_{11} + X_{33} = P$, and $X_{13} = X_{31} = -\frac{1}{3}\sqrt{2}\,P$;

$$\xi_1 = \tfrac{1}{3}P[(S_{11} + S_{12}) + S_{13}],$$

$$\xi_2 + \xi_4 = \tfrac{1}{3}P[(S_{11} - S_{12}) \pm \sqrt{2}S_{15}](\tfrac{4}{3}\cos^2\omega - 1),$$

$$\xi_3 + \xi_5 = \tfrac{2}{9}P(-S_{44} \mp \sqrt{2}\,S_{51}\cos^2\omega).$$

The shifts are given by:

$$g\mu_B\Delta H = \xi_1[A(1 - 2\cos^2\omega) - \tfrac{2}{3}B(3 - 2\cos^2\omega)\cos^2\omega - 3C(1 - \tfrac{2}{3}\cos^2\omega)^2]$$
$$+ (\xi_2 + \xi_4)[A - \tfrac{2}{3}B\cos^2\omega + C(1 + \tfrac{2}{3}\cos^2\omega)] + (\xi_3 + \xi_5)[A + \tfrac{1}{2}B(1 - \tfrac{4}{3}\cos^2\omega) - C(1 - \tfrac{2}{3}\cos^2\omega)] .$$

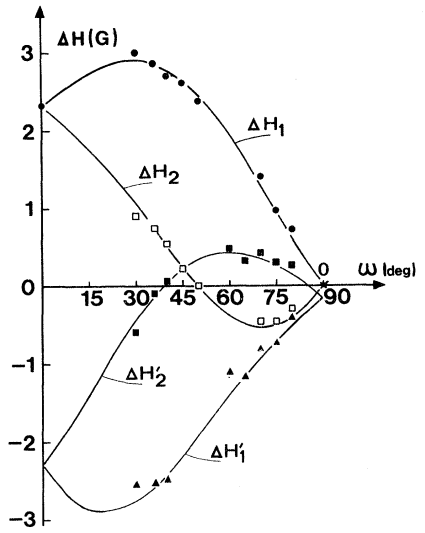

FIG. 3. ZnS:Mn^{++}. Angular variation of the values of the displacements of the lines corresponding to the transitions $M_S(-\frac{3}{2} \longleftrightarrow -\frac{5}{2})$ and $M_S(+\frac{5}{2} \longleftrightarrow +\frac{3}{2})$. ΔH_1 and $\Delta H_1'$ are the shifts corresponding to one hexagonal site. ΔH_2 and $\Delta H_2'$ are the shifts corresponding to the other hexagonal site. The dimensions of the sample were $8.25 \times 2.85 \times 1.55$ mm, the cross-sectional area perpendicular to the applied pressure was $(2.85 \pm 0.01) \times (1.55 \pm 0.01)$ mm^2; pressure was applied perpendicular to the c axis and $\vec{H}$ was rotated in a mirror plane ($P = 2 \times 10^8$ dyn/cm^2). ω is defined in Fig. 1.

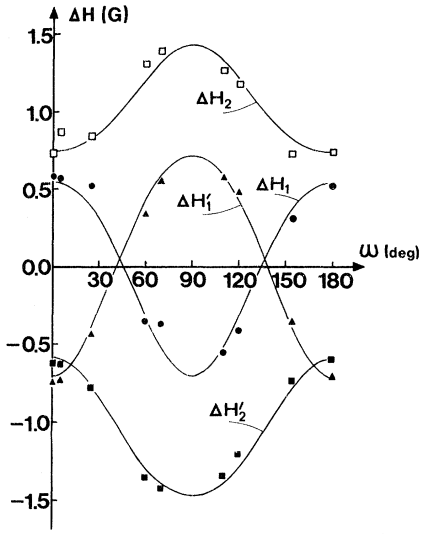

FIG. 5. Angular variation of the shifts ΔH_1 and ΔH_2 of the absorption lines $M_S(-\frac{3}{2} \longleftrightarrow -\frac{5}{2})$ ΔH_1 corresponds to one hexagonal center and ΔH_2 corresponds to the other hexagonal center). The shifts $\Delta H_1'$ and $\Delta H_2'$ of the lines $M_S(+\frac{3}{2} \longleftrightarrow +\frac{5}{2})$ are also reported in this figure. Pressure was applied in a mirror plane at 54° 44′ of the c axis ($P = 0.9 \times 10^8$ dyn/cm^2). The dimensions of the sample were $6.1 \times 2.96 \times 1.89$ mm. The cross-sectional area perpendicular to the applied pressure was $(2.96 \pm 0.01) \times (1.89 \pm 0.01)$ mm^2.

Figure 5 shows the angular variations of the shifts ΔH_1 and ΔH_2 for the two sites corresponding to the absorption lines $M_S(-\frac{3}{2} \longleftrightarrow -\frac{5}{2})$ and the shifts ΔH_2 corresponding to the absorption lines $M_S(+\frac{3}{2} \longleftrightarrow +\frac{5}{2})$. The experimental values of C_{44} and C_{15} are deduced from the angular variations of the quantities $-\frac{1}{2}(\Delta H_1' + \Delta H_2')$ (Fig. 6). [$\Delta H_1'$ and $\Delta H_2'$ correspond to the transition $M_S(+\frac{3}{2} \longleftrightarrow +\frac{5}{2})$.] We obtain

$$C_{44} = 1.4 \times 10^{-13} \text{ cm/dyn}$$

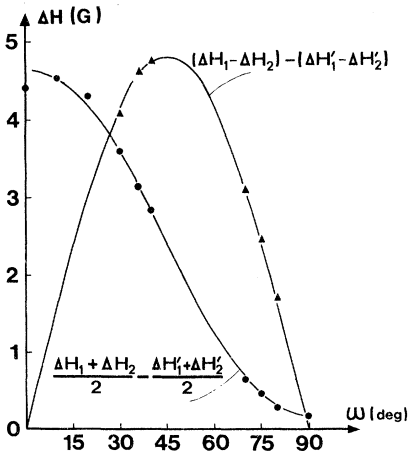

FIG. 4. Angular variations of the quantities $\frac{1}{2}(\Delta H_1 + \Delta H_2) - \frac{1}{2}(\Delta H_1' + \Delta H_2')$ and $(\Delta H_1 - \Delta H_2) - (\Delta H_1' - \Delta H_2')$. The shifts ΔH_1, ΔH_2, $\Delta H_1'$, and $\Delta H_2'$ are given in Fig. 3. The curve corresponding to $(\Delta H_1 - \Delta H_2) - (\Delta H_1' - \Delta H_2')$ is related to C_{51}, the other to C_{11} and C_{12}.

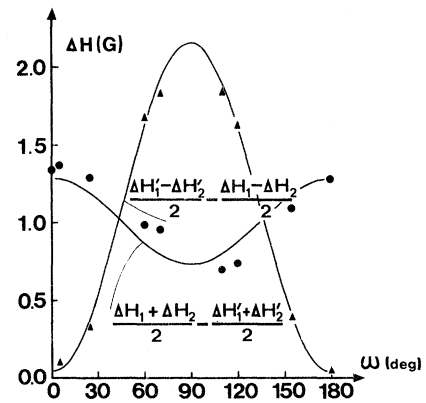

FIG. 6. Angular variation of the quantities $\frac{1}{2}(\Delta H_1' - \Delta H_2') - \frac{1}{2}(\Delta H_1 - \Delta H_2)$ and $\frac{1}{2}(\Delta H_1 + \Delta H_2) - \frac{1}{2}(\Delta H_1' + \Delta H_2')$. The shifts ΔH_1, ΔH_2, $\Delta H_1'$, and $\Delta H_2'$ are given in Fig. 5. The theoretical curve corresponding to $\frac{1}{2}(\Delta H_1' - \Delta H_2') - \frac{1}{2}(\Delta H_1 - \Delta H_2)$ gives $|C_{51}| = 0.97 \times 10^{-13}$ cm/dyn and $|C_{15}| = 1.9 \times 10^{-13}$ cm/dyn. The other theoretical curve gives $C_{44} = 1.4 \times 10^{-13}$ cm/dyn (the coefficients C_{13}, C_{11}, and C_{12} previously determined also intervene in the determination of the theoretical curve).

and

$$C_{15} = 1.9\times10^{-13} \text{ cm/dyn} .$$

IV. THEORY

The evaluation of the SLCC's in the case of cubic symmetry has been undertaken for a long time[16–20]; however, it was only recently that a detailed treatment by Sharma[8] appeared for the $3d^5$ ions in trigonal symmetry. Great emphasis was given to the Blume–Orbach (BO) mechanism, the other mechanisms like spin-spin interaction, higher-order effects proposed by Das, Orbach, and Sharma (SDO mechanism), and the Watanabe process, all being less important. However, we will evaluate the contribution of these mechanisms, also taking the pressure-induced odd crystal fields into account.

The Hamiltonian governing the $3d^5$ ions will be written

$$\mathcal{H} = \mathcal{H}_0 + V_c + \mathcal{H}_{so} + V_{odd} + \Delta V_{even} + \Delta V_{odd} ,$$

$\mathcal{H}_0$ being the free-ion Hamiltonian, V_c and $\mathcal{H}_{so}$ being, respectively, the even part of the cubic crystal field and the spin-orbit interaction. ΔV_{even} and ΔV_{odd} are, respectively, the even and odd parts of the pressure-induced crystal field. V_{odd} is the odd cubic part of the crystal field.

Our first aim will be to evaluate the contribution of ΔV_{even} to the SLCC's in the case of a C_{3v} symmetry. The most important contribution of ΔV_{even} is due to the BO mechanism, coupling the fundamental state to the optical multiplets $^4_i T_1$ by the spin-orbit interaction and by the pressure-induced even crystal field. In our case it is convenient to calculate the contribution of the most general form of ΔV_{even}, thus we will write

$$\Delta V_{even} = \sum_{k \text{ even}} B^q_k D^{(k)}_q ,$$

$D^{(k)}_q$'s being tensor operators as defined by Judd.[21] Linear combinations of the spectroscopic terms spanning the A_2 and E representations of the C_{3v} symmetry will be used here. The only advantage of this choice is to simplify the theoretical expressions obtained for the diagonal elements of the spin Hamiltonian. Several basis functions used in this paper are different from those of Sharma[8] because the phase conventions of Racah and Slater[22,23] were chosen in order to apply general relations giving matrix elements of the spin-orbit interaction and crystal field. The general expression for the $|^6SM_S\rangle$ state, perturbed by $\mathcal{H}_{so}$ and ΔV_{even} (BO process), is

$$|^6SM_S\rangle' = |^6SM_S\rangle + \sum_{i=1}^{3} \frac{\alpha_i \zeta}{\Delta_i} \Big(\langle (P)\, ^4E^+ M_S - 1 | \sum_j - \rho^1_{1,j} s^1_{-1,j} | ^6SM_S\rangle |^4_i E^+ M_S - 1\rangle$$
$$+ \langle (P)\, ^4E^- M_S + 1 | \sum_j - \rho^1_{-1,j} s^1_{1,j} | ^6SM_S\rangle |^4_i E^- M_S + 1\rangle + \langle (P)\, ^4A_2\, M_S | \sum_j \rho^1_{0,j} s^1_{0,j} | ^6SM_S\rangle |^4_i A_2 M_S\rangle \Big) .$$

In this expression, $\mathcal{H}_{so}$ is expressed in terms of the components of tensor operators whose matrix elements can be calculated from the V^{11} of Racah. The states $|^4_i E^+\rangle$, $|^4_i E^-\rangle$, and $|^4_i A_2\rangle$ span the E and A_2 representations of the group C_{3v}. α_i's are the parameters describing the mixing of the $|^4T_1\rangle$ levels by the cubic crystal field. Δ_i is the energy difference $E(^6A_1) - E(^4T_1)$. ζ is the spin-orbit constant. Following our conventions, the signs of the basis functions $|(F)\,^4E^+\rangle$, $|(F)\,^4E^-\rangle$, and $|(F)\,^4A_2\rangle$ as given by Sharma,[8] must be changed.

The G_{ijkl}'s can be calculated by comparing the matrix elements of the spin Hamiltonian $\mathcal{H}_{strain}$ with the matrix elements $\langle (^6SM_S)' | \Delta V_{even} | (^6SM'_S)' \rangle$. The spin Hamiltonian will be written

$$\mathcal{H}_{strain} = (G_{11}\epsilon_{11} + G_{12}\epsilon_{22} + 2G_{15}\epsilon_{13} + G_{13}\epsilon_{33}) S_1^2 + (G_{12}\epsilon_{11} + G_{11}\epsilon_{22} + G_{13}\epsilon_{33} - 2G_{15}\epsilon_{13})\, S_2^2$$
$$+ [-(G_{11} + G_{12})(\epsilon_{11} + \epsilon_{22}) - 2G_{13}\epsilon_{33}] S_3^2 + 2(G_{44}\epsilon_{23} - G_{51}\epsilon_{12})(S_2S_3 + S_3S_2)$$
$$+ [G_{51}(\epsilon_{11} - \epsilon_{22}) + 2G_{44}\epsilon_{13}](S_1S_3 + S_3S_1) + [-2G_{15}\epsilon_{23} + (G_{11} - G_{12})\epsilon_{12}](S_1S_2 + S_2S_1) ,$$

no factor of 2 or 4 being introduced in the definition of the G_{ijkl}'s nor in the ϵ_{ij}'s.

We will evaluate the G's by taking into account only one element of the strain tensor and then evaluating the pressure-induced crystal field operators corresponding to the chosen strain (all other strains being taken as zero). Thus, $G_{11}+G_{12}$ and G_{13} can be determined from the difference between two diagonal matrix elements.

For $\epsilon_{11} \neq 0$, we get

$$(G_{11} + G_{12})_{\epsilon_{11}\neq 0} = -\tfrac{1}{6} [\langle (\tfrac{5}{2}, \tfrac{5}{2})' | \Delta V_{even}(\epsilon_{11} \neq 0) | (\tfrac{5}{2}, \tfrac{5}{2})' \rangle$$

$$- \langle(\tfrac{5}{2}, \tfrac{3}{2})' \,|\, \Delta V_{\text{even}}(\epsilon_{11} \neq 0) \,|\, (\tfrac{5}{2}, \tfrac{3}{2})'\rangle]$$

and

$$(G_{13})_{\epsilon_{33}\neq 0} = -\tfrac{1}{12}[\langle(\tfrac{5}{2}, \tfrac{5}{2})' \,|\, \Delta V_{\text{even}}(\epsilon_{33} \neq 0) \,|\, (\tfrac{5}{2}, \tfrac{5}{2})'\rangle - \langle(\tfrac{5}{2}, \tfrac{3}{2})' \,|\, \Delta V_{\text{even}}(\epsilon_{33} \neq 0) \,|\, (\tfrac{5}{2}, \tfrac{3}{2})'\rangle] .$$

The coefficients G_{51} and G_{44} can be deduced from the nondiagonal elements $\Delta M_S \pm 1$. Taking as nonzero strains ϵ_{11} and ϵ_{13}, we get

$$(G_{51})_{\epsilon_{11}\neq 0} = \tfrac{1}{10}\sqrt{5}\,\langle(\tfrac{5}{2}, \tfrac{5}{2})' \,|\, \Delta V_{\text{even}}(\epsilon_{11} \neq 0) \,|\, (\tfrac{5}{2}, \tfrac{3}{2})'\rangle$$

and

$$(G_{44})_{\epsilon_{13}\neq 0} = \tfrac{1}{20}\sqrt{5}\,\langle(\tfrac{5}{2}, \tfrac{5}{2})' \,|\, \Delta V_{\text{even}}(\epsilon_{13} \neq 0) \,|\, (\tfrac{5}{2}, \tfrac{3}{2})'\rangle .$$

The other G coefficients can be deduced from nondiagonal terms $\Delta M_S = \pm 2$,

$$(G_{15})_{\epsilon_{13}\neq 0} = (1/\sqrt{40})\,\langle(\tfrac{5}{2}, \tfrac{5}{2})' \,|\, \Delta V_{\text{even}}(\epsilon_{13} \neq 0) \,|\, (\tfrac{5}{2}, \tfrac{1}{2})'\rangle,$$

$$(G_{11} - G_{12})_{\epsilon_{11}\neq 0} = (4/\sqrt{40}) \times \langle(\tfrac{5}{2}, \tfrac{5}{2})' \,|\, \Delta V_{\text{even}}(\epsilon_{11} \neq 0) \,|\, (\tfrac{5}{2}, \tfrac{1}{2})'\rangle.$$

The next task is to calculate the matrix elements $\langle(SM_S)' \,|\, \Delta V_{\text{even}} \,|\, (S'M'_S)'\rangle$. It is easy to verify that the difference of matrix elements giving $G_{11} - G_{12}$ and G_{13} is analogous to an expression given by Sharma,[8] thus by choosing the relevant strains, we get

$$\begin{aligned} G_{11} + G_{12} &= \tfrac{2}{14}\sqrt{5}\,(B_2^0)_{\epsilon_{11}\neq 0}\langle r^2\rangle \zeta^2 p\alpha\beta p\alpha\gamma \\ &\quad - \tfrac{2}{189}\sqrt{5}\,(B_4^0)'_{\epsilon_{11}\neq 0}\langle r^4\rangle \zeta^2 p\alpha\gamma\,(7p\alpha\alpha + 4p\alpha\beta) , \\ G_{13} &= \tfrac{1}{14}\sqrt{5}\,(B_2^0)_{\epsilon_{33}\neq 0}\langle r^2\rangle \zeta^2 p\alpha\beta\, p\alpha\gamma \\ &\quad - \tfrac{1}{189}\sqrt{5}\,(B_4^0)'_{\epsilon_{33}\neq 0}\langle r^4\rangle \zeta^2 p\alpha\gamma\,(7p\alpha\alpha + 4p\alpha\beta) , \end{aligned} \tag{1}$$

with $(B_4^0)' = B_4^0 - (\sqrt{7}/\sqrt{10})B_4^{-3}$ and $\langle r^k\rangle = \langle 3d^5 \,|\, r^k \,|\, 3d^5\rangle$,

$$p\alpha\alpha = \sum \alpha_i^2/\Delta_i , \quad p\alpha\beta = \sum \alpha_i\beta_i/\Delta_i ,$$

and

$$p\alpha\gamma = \sum \alpha_i\gamma_i/\Delta_i ,$$

α_i, β_i, γ_i being the coefficients governing the mixing of the multiplets. It is important to note that $D^{(2)}$ and $D^{(4)}$ are the only crystal field operators which intervene in the calculation of the diagonal matrix elements.

Other crystal field operators appear in the nondiagonal terms. Using the following reduced matrix elements of the tensor operators $D_q^{(2)}$ and $D_q^{(4)}$ acting between spectroscopic terms $|L, M_L\rangle$ and $|L', M_{L'}\rangle$,

$$\langle 4\|D^{(2)}\|3\rangle = -\langle 3\|D^{(2)}\|4\rangle = 30/7\sqrt{4\pi} ,$$

$$\langle 4\|D^{(4)}\|3\rangle = -\langle 3\|D^{(4)}\|4\rangle = -3\sqrt{110}/7\sqrt{4\pi} ,$$

$$\langle 4\|D^{(4)}\|1\rangle = -\langle 1\|D^{(4)}\|4\rangle = 3\sqrt{140}/7\sqrt{4\pi} ,$$

we get

$$\begin{aligned} \langle(\tfrac{5}{2}, \tfrac{5}{2})' \,|\, \Delta V_{\text{even}} \,|\, (\tfrac{5}{2}, \tfrac{3}{2})'\rangle &= +\tfrac{5}{21}\sqrt{6}B_2^1\lambda + \tfrac{8}{63}\sqrt{20}B_4^1\mu \\ &\quad - \tfrac{1}{18}\sqrt{20}B_4^1\nu - \tfrac{10}{21}\sqrt{3}B_2^{-2}\lambda - \tfrac{10}{63}\sqrt{20}\,B_4^{-2}\mu + \tfrac{5}{18}\sqrt{20}B_4^2\nu \\ &\quad + \tfrac{1}{9}\sqrt{140}\,B_4^4\nu - \tfrac{8}{189}\sqrt{140}B_4^4\mu \end{aligned} \tag{2}$$

and

$$\begin{aligned} \langle(\tfrac{5}{2}, \tfrac{5}{2})' \,|\, \Delta V_{\text{even}} \,|\, (\tfrac{5}{2}, \tfrac{1}{2})'\rangle &= -\tfrac{1}{3}\sqrt{5}\,B_4^2\nu + \tfrac{8}{63}\sqrt{5}\,B_4^2\lambda \\ &\quad - \tfrac{1}{3}\sqrt{5}B_4^{-1}\nu - \tfrac{2}{63}\sqrt{5}B_4^{-1}\mu - (10/7\sqrt{3})B_2^2\lambda \\ &\quad - (5\sqrt{2}/7\sqrt{3})B_2^{-1}\lambda + (5\sqrt{5}/9\sqrt{7})B_4^{-4}\mu , \end{aligned} \tag{3}$$

with

$$\begin{aligned} \lambda &= \langle r^2\rangle \zeta^2\, p\alpha\beta\, p\alpha\gamma , \\ \mu &= \langle r^4\rangle \zeta^2\, p\alpha\beta\, p\alpha\gamma , \\ \nu &= \langle r^4\rangle \zeta^2\, p\alpha\gamma\, p\alpha\alpha . \end{aligned} \tag{4}$$

In each case, it is necessary to calculate the crystal field amplitude corresponding to the chosen nonzero strain and then to apply the above formulas in order to calculate the G_{ij}'s. The amplitude of the crystal fields must be calculated in a trigonal axis system (x, y, z). In order to relate directly the matrix elements of ΔV_{even} with the matrix elements of the spin Hamiltonians of Sec. II, $\vec{x}$ must be in a mirror plane and $\vec{z}$ must be along the c axis.

The higher-order effects such as the Watanabe mechanism, SDO mechanism, and spin-spin mechanism will be considered in Sec. V. The contribution of the first two effects is negligible in our case, and the contribution due to the spin-spin mechanism does not exceed 10% of the value obtained from the BO mechanism. Therefore, we will consider a new mechanism which was not studied in previous papers, that is, the internal-odd-fields contribution by intermediary of opposite-parity excited-configuration $3d^4\,4p$ and $3d^4\,4f$. The method of equivalent even field operators will be used here. First developed by Kiel[24] following a perturbation procedure given by Judd[21] and Ofelt,[25] this method was applied in a preceding paper[26] in which we also demonstrated the importance of the mixing of the quadruplets $^4T_1$ by the even cubic part of the crystal field. The same procedure can be generalized to the case treated here. The pressure-induced crystal field is written in the form

$$V = \sum_{t,p} B_t^p D_p^{(t)} ,$$

giving the general expression for the equivalent even field

$$V_{\text{equ}} = 2\sum_{t,p}\sum_n{}' B_k^q B_t^p \,\frac{D_q^{(k)}\,|\psi_n\rangle\langle\psi_n|D_p^{(t)}}{E_0 - E_n} ,$$

where E_n is the energy of an excited configuration $3d^4\,4p$ or $3d^4\,4f$, assumed well separated from the fundamental configuration. $|\psi_n\rangle$'s are states is-

sued from the excited configurations of odd parity.

The equivalent even operator obtained by summing on all relevant quantum numbers defining the states $|\psi_n\rangle$ is given in a preceding paper.[26] The explicit form of the equivalent even crystal field is

$$V_{\text{equ}} = 2\sum_{\lambda}\sum_{t,p}\sum_{(n'\rho')}(1)^{p+q}[\lambda][\rho']\begin{pmatrix} k & \lambda & t \\ q & -p-q & p\end{pmatrix}$$

$$\times\begin{Bmatrix} k & \lambda & t \\ \rho & \rho' & \rho\end{Bmatrix}\begin{pmatrix} \rho & k & \rho' \\ 0 & 0 & 0\end{pmatrix}\begin{pmatrix} \rho' & t & \rho \\ 0 & 0 & 0\end{pmatrix}\begin{pmatrix} \rho & \lambda & \rho \\ 0 & 0 & 0\end{pmatrix}^{-1}$$

$$\times\frac{\langle n\rho|r^k|n'\rho'\rangle\langle n\rho|r^t|n'\rho'\rangle}{\langle n\rho|r^\lambda|n\rho\rangle}\frac{B_k^q B_t^q}{E_{(n'\rho')}-E_{(n\rho)}}D_{p+q}^{(\lambda)}$$

(the notations are those of Judd[21]).

In the chosen axis system, the internal crystal field of odd parity is given in terms of $B_3^0 D_0^{(3)}$, $B_3^{-3}D_{-3}^{(3)}$, and $B_3^3 D_3^{(3)}$; thus, the excited configuration $3d^4 4p$ act on the SLCC's by intermediary of the pressure-induced odd fields in $B_1^q D_q^{(1)}$ and $B_3^q D_q^{(3)}$. In order to study the influence of the $3d^4 4f$ configuration, it is also necessary to take into account the odd fields $B_5^q D_q^{(5)}$. We shall neglect here this configuration because the mean value $\langle n\rho|r^k|n'\rho'\rangle$ (k given) is much smaller for excited configurations $3d^4 4f$ than for excited configurations $3d^4 4p$, at least for Mn^{++}.

The contribution of the $3d^4 4p$ configuration to the SLCC's can be easily deduced from the general formulas given in this section and from the amplitudes of the equivalent crystal field given in the appendix.

V. RESULTS AND DISCUSSION

A. Stacking Faults in ZnS

Since the structure of the two sites studied is not defined exactly, we will perform the calculations for all the probable sites[11] and compare the theoretical results with the experiments. Our samples presented, simultaneously, two cubic centers related by a rotation of 180° around the [111] crystallographic axis and four axial sites, two of them being those studied experimentally and the two others corresponding to an axial-field parameter $D = +36.1\times10^{-4}$ cm^{-1}.[11] Two axial centers having the same parameter D are related by a rotation of 180° around the [111] crystallographic axis. Since our samples were predominantly cubic, we will consider the axial sites as being in the neighborhood of a stacking fault which could also explain the presence of the two cubic centers.

We will make the hypothesis that the axial sites existing in our samples are due to the sequence of ZnS layers[27] *ABCACB*, this being the simplest stacking fault to explain the presence of all the sites in our sample. The different sites appearing in this sequence can be conveniently described by the position of the first, second, and third neighbors.[11] Two sites denoted *AS* possess six second neighbors forming a trigonal antiprism and one third neighbor on the [111] axis. Two other sites possess six second neighbors forming a trigonal prism without a third neighbor on the [111] axis. These sites are denoted *PN*. Two sites showing the same structure as in the cubic phase up to the third neighbors will be not considered here.

We will also consider the case of Mn^{++} in wurtzite although this structure does not appear in our EPR spectra ($D = -98.8\times10^{-4}$ cm^{-1} [28]).

B. Blume and Orbach Mechanism

The parameters α_i, β_i, γ_i were calculated from the energy levels of Mn^{++} in sphalerite but, instead of taking the best fit for the $^4T_1$ level alone, we deduced the Racah parameters and the cubic field parameter from the best fitting for all levels $^4T_1$, $^4T_2$, and ^4E. The values are

$$B = 730\ \text{cm}^{-1},\quad C = 2880\ \text{cm}^{-1},\quad Dq = -420\ \text{cm}^{-1}.$$

These values give $p\alpha\alpha = 44.09\times10^{-6}$ cm, $p\alpha\beta = -0.3607\times10^{-6}$ cm, and $p\alpha\gamma = -7.463\times10^{-6}$ cm. Other values intervening in the calculation are $\zeta = 300$ cm^{-1}, $\langle 3d|r^2|3d\rangle = 1.548\ a_0^2$,[9] $\langle 3d|r^4|3d\rangle = 5.5126\ a_0^4$[9] ($a_0$ being the first Bohr radius), and $R = 2.35$ Å.[27]

The pressure-induced crystal field was calculated in a point-charge model. The values of the components of the pressure-induced even crystal field and their contribution to the G_{ijkl}'s for wurtzite and for the sites *AS* and *PN* are given in Tables I and II. It clearly appears that the components of rank four of the crystal potential give the preponderant contribution to the G's. This fact can be simply related to the very high value of the parameter ν compared to λ and μ [see formula (4)],

$$\nu = -16,\ 325.7\times10^{-8}\ a_0^4,$$

$$\mu = 133.56\times10^{-8}\ a_0^4,\qquad \lambda = 37.50\times10^{-8}\ a_0^2.$$

Thus, an examination of the relations (1)–(4) given in Sec. IV shows that the important contributions are due to B_4^0 for $G_{11}+G_{12}$; B_4^1, $B_4^{\pm2}$, and B_4^4 for G_{51} and G_{44}; B_4^2 and B_4^{-1} for $G_{11}-G_{12}$ and G_{15}. The contribution of the crystal potentials in $B_2^q D_q^{(2)}$ is at most $\frac{1}{100}$th of the experimental values of the G's, therefore, in the BO scheme, these potentials do not intervene significantly in the calculation of the G's of Mn^{++} in wurtzite and in sites *AS* and *PN*.

In order to compare the experimental and theoretical values, it is necessary to calculate the tensor $\underline{C}$ from the tensor $\underline{G}$ and the elasticity tensor $\underline{s}$. From the following contracted tensor multiplication

$$G_{ijkl}\,s_{klrs} = C_{ijrs},$$

TABLE I. Amplitudes of the components of the pressure-induced crystal fields in a point-charge approximation. The indices ij of the ϵ's mean that ϵ_{ij} is the only strain responsible for the amplitude, other strains being zero. The values given permit the calculation of the G's as given in the left column. The B_k^q's are in units of $e^2/2a_0^{k+1}$ (a_0 is the first Bohr radius).

	Wurtzite		*AS* and *PN* (values for PN are given in parentheses)
$G_{11}+G_{12}$	$(B_2^0)_{\epsilon_{11}} = +0.131\,04$	$G_{11}+G_{12}$	$(B_2^0)_{\epsilon_{11}} = +0.131\,04$
	$(B_4^0)'_{\epsilon_{11}} = +0.106\,84$		$(B_4^0)'_{\epsilon_{11}} = +0.106\,84$
G_{13}	$(B_2^0)_{\epsilon_{33}} = -0.390\,89$	G_{13}	$(B_2^0)_{\epsilon_{33}} = -0.390\,89$ $(-0.262\,11)$
	$(B_4^0)'_{\epsilon_{33}} = -0.210\,61$		$(B_4^0)_{\epsilon_{33}} = -0.196\,12$ $(-0.200\,17)$
G_{51}	$(B_2^{-2})_{\epsilon_{11}} = -0.026\,74$	G_{51}	$(B_2^{-2})_{\epsilon_{11}} = -0.026\,74$
$G_{11}-G_{12}$	$(B_2^1)_{\epsilon_{11}} = +0.255\,02$	$G_{11}-G_{12}$	$(B_2^1)_{\epsilon_{11}} = +0.189\,14$
	$(B_4^1)_{\epsilon_{11}} = -0.044\,04$		$(B_4^1)_{\epsilon_{11}} = -0.050\,44$
	$(B_4^2)_{\epsilon_{11}} = -0.011\,77$		$(B_4^2)_{\epsilon_{11}} = -0.011\,77$
	$(B_4^4)_{\epsilon_{11}} = -0.082\,31$		$(B_4^4)_{\epsilon_{11}} = -0.082\,31$
G_{44},	$(B_2^{-2})_{\epsilon_{13}} = -0.509\,79$	G_{44},	$(B_2^{-2})_{\epsilon_{13}} = -0.378\,09$
G_{15}	$(B_2^1)_{\epsilon_{13}} = -0.266\,79$	G_{15}	$(B_2^1)_{\epsilon_{13}} = -0.266\,79$ $(-0.214\,163)$
	$(B_4^1)_{\epsilon_{13}} = -0.127\,49$		$(B_4^1)_{\epsilon_{13}} = -0.127\,49$ $(-0.122\,83)$
	$(B_4^{-2})_{\epsilon_{13}} = +0.062\,29$		$(B_4^{-2})_{\epsilon_{13}} = +0.086\,43$
	$(B_4^4)_{\epsilon_{13}} = -0.047\,08$		$(B_4^4)_{\epsilon_{13}} = -0.048\,22$

we get

$$C_{11} + C_{12} = (G_{11} + G_{12})(s_{11} + s_{12}) + 2G_{13}s_{13} ,$$

$$C_{11} - C_{12} = (G_{11} - G_{12})(s_{11} - s_{12}) + 2G_{15}s_{51} ,$$

$$C_{44} = \tfrac{1}{2}G_{44}s_{44} + G_{51}s_{51} ,$$

$$C_{51} = G_{51}(s_{11} - s_{12}) + G_{44}s_{15} ,$$

$$C_{13} = (G_{11} + G_{12})s_{13} + G_{13}s_{33} ,$$

$$C_{15} = \tfrac{1}{2}G_{15}s_{44} + (G_{11} - G_{12})s_{15} .$$

The notations of the tensors $\underline{C}$ and $\underline{G}$ are defined in Sec. II and IV. The s_{ij}'s are the same as those defined by Nye[13] and Bhagavantam.[14] In the above relations the s_{ij}'s are the elastic compliance constants of cubic ZnS. They are expressed in the axis system defined in Sec. II. The above relations will be used in the calculation of the deformations of the sites *PN* and *AS*. The elastic compliance constants for cubic ZnS were measured by Berlincourt *et al.*[29] In our axis system we get

$$s_{12} = -0.463\times10^{-12}\ \text{cm}^2/\text{dyn} ,$$

$$s_{11} = +1.108\times10^{-12}\ \text{cm}^2/\text{dyn} ,$$

$$s_{44} = +4.117\times10^{-12}\ \text{cm}^2/\text{dyn} ,$$

$$s_{13} = -0.219\times10^{-12}\ \text{cm}^2/\text{dyn} ,$$

$$s_{33} = +0.864\times10^{-12}\ \text{cm}^2/\text{dyn} ,$$

$$s_{15} = -0.689\times10^{-12}\ \text{cm}^2/\text{dyn} .$$

These values were taken at 25 °C, the average temperature coefficients are less than 10^{-4}/°C.

The elastic compliance constants of wurtzite were recently measured in terms of temperature by Kobyakov and Pado.[30] At room temperatures, they are

$$s_{12} = -0.434\times10^{-12}\ \text{cm}^2/\text{dyn} ,$$

$$s_{11} = +1.113\times10^{-12}\ \text{cm}^2/\text{dyn} ,$$

$$s_{44} = +3.428\times10^{-12}\ \text{cm}^2/\text{dyn} ,$$

$$s_{13} = -0.148\times10^{-12}\ \text{cm}^2/\text{dyn} ,$$

$$s_{33} = +0.853\times10^{-12}\ \text{cm}^2/\text{dyn} .$$

As in cubic ZnS these values vary slightly with the temperature between 1.5 and 300 °K. The relative variation of the s_{ij} is roughly 3% for s_{13}, 2% for s_{55}, s_{11}, and s_{33}; and 1% for s_{12}. Therefore, the temperature dependence of the C coefficients should hardly be observed by experiments (the variation of the crystal field by thermal dilatation being neglected).

The experimental and theoretical values of the C_{ij}'s are given in Tables III and IV. It appears that for the sites *AS* and *PN* the theoretical values are roughly identical. When compared to the experimental results the values of C_{11}, C_{51}, C_{13}, and C_{15} are of correct magnitude but the coefficients C_{12} and C_{44} are in disagreement. From the formulas giving $C_{11}+C_{12}$ and $C_{11}-C_{12}$ it is clear that the theoretical results should be more precise than the results we were able to obtain from our model to get the correct sign for C_{12}. Therefore, the wrong sign for C_{12} is not surprising. It is not yet understood however, why there is a wrong sign for C_{44}. There being no significant differences in the theoretical C_{ij}'s, we cannot attribute the axial centers studied experimentally to Mn^{++} in either *PN* or *AS* sites.

C. Other Mechanisms

The Watanabe process[31] can be generalized to our case by remarking that the following terms linear in P,

$$\frac{\langle {}^6S|\mathcal{H}_{so}|{}^4P\rangle\langle {}^4P|V_{even}|{}^4D\rangle\langle {}^4D|(\Delta V_{even})_{ij}|{}^4P\rangle\langle {}^4P|\mathcal{H}_{so}|{}^6S\rangle + \text{c. c.}}{(E\,{}^6S - E\,{}^4P)^2(E\,{}^6S - E\,{}^4D)} ,$$

contribute to the G's. It can be easily seen that only crystal potentials in $B_2^q D_q^{(2)}$ will intervene in the above expression. In the case of Mn^{++} in wurtzite, the amplitude of the crystal potentials of

TABLE II. Contribution of the crystal fields $V_q^{(k)}$ to the coefficients G_{ij}. Numerical values are given in units of cm^{-1} per unit strain.

Crystal field	Wurtzite $G_{11}+G_{12}$	Wurtzite G_{13}	*AS* and *PN* (values for *PN* are given in parentheses) $G_{11}+G_{12}$	*AS* and *PN* (values for *PN* are given in parentheses) G_{13}
$V_0^{(2)}$	+0.001 76	−0.002 57	+0.001 76	−0.002 57 (−0.001 72)
$V_0^{(4)}$,	+0.315 44	−0.310 88	+0.315 44	−0.289 49 (−0.295 47)
	G_{51}	G_{44}	G_{51}	G_{44}
$V_{-2}^{(2)}$	+0.000 20	+0.001 93	+0.000 20	+0.001 43
$V_1^{(2)}$	+0.001 37	−0.000 72	+0.001 02	−0.000 72 (−0.000 58)
$V_1^{(4)}$	−0.044 64	−0.064 56	−0.051 12	−0.064 56 (−0.062 16)
$V_{\pm 2}^{(4)}$	+0.058 83	−0.155 65	+0.058 83	−0.215 97
$V_4^{(4)}$	+0.433 83	+0.124 08	+0.433 83	+0.127 08
	$G_{11}-G_{12}$	G_{15}	$G_{11}-G_{12}$	G_{15}
$V_2^{(4)}$	−0.099 67	+0.131 64	−0.099 67	+0.182 66
$V_{-1}^{(4)}$	+0.371 49	+0.267 26	+0.425 46	+0.267 26 (+0.257 49)
$V_2^{(2)}$	+0.000 57	+0.002 73	+0.000 57	+0.002 02
$V_4^{(4)}$	−0.003 58	−0.000 51	−0.003 58	−0.000 52
$V_{-1}^{(2)}$	+0.003 67	−0.000 99	+0.002 72	−0.000 99 (−0.000 80)

rank two is small, thus, in the axis system chosen in this paper, the only term different from zero is $B_2^0 = -0.000\,73\, e^2/2a_0^3$. The contribution of this mechanism to the G's is less than 10^{-4} cm^{-1} per unit strain and therefore negligible in our case.

Given the small value of B_2^0, the influence of the generalized Das, Orbach, and Sharma mechanism describing the influence of configurationally admixed even wave functions can also be neglected; the contribution to the G's being of the order of 10^{-4} cm^{-1} per unit strain.

Therefore, in the case of Mn^{++} in wurtzite and in the sites *PN* and *AS*, the mechanisms bilinear in $(B_2^0)_{crystal}$ and $(B_2^q)_{ij}$ can be neglected; this fact being due primarily to the smallness of the $(B_2^0)_{crystal}$.

In our case, the spin-spin mechanism gives a non-negligible contribution. Its contribution to the diagonal terms of the spin Hamiltonian has been studied by Sharma.[9] Using the results of Sharma it can be easily found that for Mn^{++} in wurtzite its contribution to $G_{11}+G_{12}$ and to G_{13} is

TABLE III. Experimental and theoretical values (BO mechanism) of the coefficients C_{ij}. All values are given in units of 10^{-13} cm/dyn. Precision of the experimental values is given in parentheses. The sites *AS* and *PN* are defined in Sec. V A.

	Sites *PN*	Sites *AS*	Experimental value	
C_{11}	+1.20	+1.09	+1.9	(10%)
C_{12}	+1.20	+2.18	∼−0.06	
C_{51}	+7.98	+8.02	+0.97	(10%)
C_{13}	−3.26	−3.22	−1.8	(10%)
C_{44}	−6.14	−6.17	+1.4	(10%)
C_{15}	+6.83	+7.03	+1.9	(5%)

TABLE IV. Theoretical values of the coefficients C_{ij} of Mn^{++} in wurtzite. All values are given in units of 10^{-13} cm/dyn.

	Contribution of the even fields (BO mechanism)	Contribution of the equivalent even fields of rank four	Theoretical value
C_{11}	+3.65	−0.91	+2.74
C_{12}	−0.57	−0.11	−0.68
C_{51}	+6.96	+1.20	+8.16
C_{13}	−3.14	+0.30	−2.84
C_{44}	−1.63	+0.84	−0.79
C_{15}	+6.86	+0.89	+7.75

$(G_{11} + G_{12})_{\text{spin-spin}} = -0.01932$ cm^{-1} per unit strain,

$(G_{13})_{\text{spin-spin}} = +0.025853$ cm^{-1} per unit strain.

Therefore, this effect is not negligible although it does not modify strongly the values obtained by using the BO mechanism.

To our knowledge, the influence of the pressure-induced fields of odd parity has not been studied previously. It clearly appears, for the same reasons given in the study of the influence of the even fields, that the contribution of the equivalent even fields of rank two is negligible compared to the influence of the equivalent fields of rank four. These fields have been calculated in a point-charge model for Mn^{++} in wurtzite. The results given in Table IV were calculated from formulas given in Sec. IV with $\mathcal{F}(3, 3, 4) = +7.55$ in units of $2a_0^3/e^2$ and $\mathcal{F}(3, 1, 4) = +1.81$ in units of $2a_0/e^2$.

D. Discussion

It must be noted that for Mn^{++} in sites *PN* or *AS*, we have neglected any local deformation not described by the strain tensor of cubic ZnS. This is a useful approximation which gives good results for simple crystal structures.[4,5,6] Of course, the validity of theoretical results depends on the validity of this approximation. Moreover, in Sec. III B, we made the additional assumption that the nearest neighbors have the same position as in cubic ZnS. This is a very crude and possibly erroneous hypothesis, but we must underscore that this hypothesis is not as essential in the calculation of the C_{ij}'s as in the calculation of the axial-field parameter, at least for the BO mechanism. In any case, the theoretical model is not sufficiently accurate to permit a definite identification of the axial sites studied experimentally, but suggests that the C_{ij}'s should be roughly identical for the sites *AS* and *PN*.

ACKNOWLEDGMENTS

Thanks are due to N. Machorine, F. Buraud, and P. Villermet for cutting the samples used in the experiments.

APPENDIX

We indicate below the amplitude of the equivalent even fields due to the composition of internal crystal fields and pressure-induced odd fields. Only equivalent even fields due to the interaction of the fundamental configuration $3d^5$ with the excited configuration $3d^4 4p$ are considered. The indices i and j mean that the B_i^p's given in brackets are related to the component ij of the strain tensor ϵ:

$$(B_0^0)_{\text{equ}(4p)} = -\tfrac{36}{35} B_3^0 (B_1^0)_{ij} \mathcal{F}(3, 1, 4) + \tfrac{54}{245} B_3^3 (B_3^{-3})_{ij} \mathcal{F}(3, 3, 4) - \tfrac{54}{245} B_3^0 (B_3^0)_{ij} \mathcal{F}(3, 3, 4) - \tfrac{36}{35} B_1^0 (B_3^0)_{ij} \mathcal{F}(3, 1, 4),$$

$$(B_4^1)_{\text{equ}(4p)} = -\tfrac{9}{35}\sqrt{10}\, B_3^0 (B_1^1)_{ij} \mathcal{F}(3, 1, 4) - \tfrac{9}{35}\sqrt{15} B_3^0 (B_3^1)_{ij} \mathcal{F}(3, 3, 4) + \tfrac{9}{245}\sqrt{30}\, B_3^3 (B_3^{-2})_{ij} \mathcal{F}(3, 3, 4) - \tfrac{9}{35}\sqrt{15}\, B_1^0 (B_3^1)_{ij} \mathcal{F}(3, 1, 4),$$

$$(B_4^2)_{\text{equ}(4p)} = +\tfrac{9}{245}\sqrt{3}\, B_3^0 (B_3^2)_{ij} \mathcal{F}(3, 3, 4) + \tfrac{27}{245}\sqrt{2}\, B_3^3 (B_3^{-1})_{ij} \mathcal{F}(3, 3, 4) - \tfrac{9}{35} B_3^3 (B_1^{-1})_{ij} \mathcal{F}(3, 1, 4) - \tfrac{18}{35}\sqrt{3}\, B_1^0 (B_3^2)_{ij} \mathcal{F}(3, 1, 4),$$

$$(B_4^3)_{\text{equ}(4p)} = +\tfrac{27}{245}\sqrt{7}\, B_3^0 (B_3^3)_{ij} \mathcal{F}(3, 3, 4) + \tfrac{27}{245}\sqrt{7}\, B_3^3 (B_3^0)_{ij} \mathcal{F}(3, 3, 4) - \tfrac{9}{35}\sqrt{7}\, B_3^3 (B_1^0)_{ij} \mathcal{F}(3, 1, 4),$$

$$(B_4^4)_{\text{equ}(4p)} = -\tfrac{18}{35}\sqrt{7} B_3^3 (B_1^1)_{ij} \mathcal{F}(3, 1, 4) + \tfrac{9}{245}\sqrt{42} B_3^3 (B_3^1)_{ij} \mathcal{F}(3, 3, 4),$$

with

$$\mathcal{F}(3, 3, 4) = \frac{(\langle 3d | r^3 | 4p \rangle)^2}{\langle 3d | r^4 | 4p \rangle} \quad \frac{-1}{E(3d) - E(4p)}$$

and

$$\mathcal{F}(3, 1, 4) = \frac{\langle 3d | r^3 | 4p \rangle \langle 3d | r | 4p \rangle}{\langle 3d | r^4 | 4p \rangle} \quad \frac{-1}{E(3d) - E(4p)}.$$

We also give the contribution of the $3d^4 4p$ excited configurations to the equivalent even terms in B_2^q:

$$(B_2^2)_{\text{equ}(4p)} = +\tfrac{36}{245}\sqrt{5} B_3^0 (B_3^2)_{ij} \mathcal{F}(3, 3, 2) + \tfrac{6}{105}\sqrt{15} B_3^3 (B_1^{-1})_{ij} \mathcal{F}(3, 1, 2) - \tfrac{18}{245}\sqrt{10} B_3^3 (B_3^{-1})_{ij} \mathcal{F}(3, 3, 2) - \tfrac{2}{35}\sqrt{5} B_1^0 (B_3^2)_{ij} \mathcal{F}(3, 1, 2),$$

$$(B_2^1)_{\text{equ}(4p)} = +\tfrac{6}{105}\sqrt{3} B_3^0 (B_1^1)_{ij} \mathcal{F}(3, 1, 2) - \tfrac{18}{245}\sqrt{2}\, B_3^0 (B_3^1)_{ij} \mathcal{F}(3, 3, 2) - \tfrac{18}{49} B_3^3 (B_3^{-2})_{ij} \mathcal{F}(3, 3, 2) - \tfrac{7}{15}\sqrt{3} B_1^0 (B_1^1)_{ij} \mathcal{F}(1, 1, 2) - \tfrac{4}{35}\sqrt{2} B_1^0 (B_3^1)_{ij} \mathcal{F}(3, 1, 2),$$

$$(B_2^0)_{\text{equ}(4p)} = -\tfrac{6}{35} B_3^0 (B_1^0)_{ij} \mathcal{F}(3,1,2) - \tfrac{72}{245} B_3^0 (B_3^0)_{ij} \mathcal{F}(3,3,2) - \tfrac{36}{49} B_3^3 (B_3^3)_{ij} \mathcal{F}(3,3,2) - \tfrac{2}{15}\sqrt{7}\, B_1^0 (B_1^0)_{ij} \mathcal{F}(1,1,2) - \tfrac{6}{35} B_1^0 (B_3^0)_{ij} \mathcal{F}(3,1,2) ,$$

where $\mathcal{F}(k, \rho, 2)$ are similar to the $\mathcal{F}(k, \rho, 4)$ but replacing $\langle 3d | r^4 | 3d \rangle$ by $\langle 3d | r^2 | 3d \rangle$.

[1]E. R. Feher, Phys. Rev. 136, A145 (1964).
[2]E. R. Feher and M. D. Sturge, Phys. Rev. **172**, 244 (1968).
[3]R. Calvo, C. Fainstein, S. B. Oseroff, and M. C. Terrile, Phys. Lett. A **30**, 287 (1969).
[4]R. R. Sharma, T. P. Das, and R. Orbach, Phys. Rev. **149**, 257 (1966).
[5]R. R. Sharma, T. P. Das, and R. Orbach, Phys. Rev. **155**, 338 (1967).
[6]R. R. Sharma, T. P. Das, and R. Orbach, Phys. Rev. **171**, 378 (1968).
[7]P. S. Han, T. P. Das, and M. F. Rettig, J. Chem. Phys. **56**, 3861 (1972).
[8]R. R. Sharma, Phys. Rev. B **3**, 76 (1971).
[9]M. Blume and R. Orbach, Phys. Rev. **127**, 5 (1962).
[10]J. Schneider, S. R. Sircar, and A. Räuber, Z. Naturforsch. A **18**, 980 (1963).
[11]T. Buch, B. Clerjaud, B. Lambert, and P. Kovacs, Phys. Rev. B (to be published).
[12]F. S. Ham, NATO Summer Course on Paramagnetic Defects in Crystals, University of Ghent, Belgium, 1967 (unpublished).
[13]J. F. Nye, *Physical Properties of Crystals* (Clarendon, Oxford, England, 1957).
[14]S. Bhagavantam, *Crystal Symmetry and Physical Properties* (Academic, New York, 1966).
[15]J. H. M. Thornley and D. Smith, Proc. Phys. Soc. Lond. **89**, 779 (1966).
[16]M. H. L. Pryce, Phys. Rev. **80**, 1107 (1950).
[17]H. Watanabe, Prog. Theor. Phys. **18**, 405 (1957).
[18]A. M. Leushin, Fiz. Tverd. Tela **5**, 605 (1963) [Sov. Phys.-Solid State **5**, 440 (1963)].
[19]J. Kondo, Prog. Theor. Phys. **28**, 1026 (1962).
[20]R. R. Sharma, Phys. Rev. **176**, 467 (1968).
[21]B. R. Judd, Phys. Rev. **127**, 750 (1962).
[22]G. Racah, Phys. Rev. **63**, 367 (1943).
[23]J. C. Slater, *Quantum Theory of Atomic Structures* (McGraw-Hill, New York, 1960), Vol. 2.
[24]A. Kiel, Phys. Rev. **148**, 247 (1966).
[25]G. S. Ofelt, J. Chem. Phys. 37, 511 (1962).
[26]R. Parrot and C. Blanchard, Phys. Rev. B 5, 819 (1972).
[27]M. Aven and J. S. Prener, *Physics and Chemistry of II-VI Compounds* (North-Holland, Amsterdam, 1967).
[28]S. P. Keller, I. L. Gelles, and W. V. Smith, Phys. Rev. **110**, 850 (1958).
[29]Don Berlincourt, H. Jaffe, and L. R. Shiozawa, Phys. Rev. **129**, 1009 (1963).
[30]I. B. Kobyakov and G. S. Pado, Fiz. Tverd. Tela **9**, 2173 (1967) [Sov. Phys.-Solid State **9**, 1707 (1968)].
[31]H. Watanabe, Prog. Theor. Phys. **18**, 405 (1957).

PHYSICAL REVIEW B VOLUME 7, NUMBER 9 1 MAY 1973

Measurement of Temperature-Dependent Correlations by Electron-Spin Resonance: Application to $Cu(NH_3)_4SO_4 \cdot H_2O$ †

Michael J. Hennessy
Department of Physics, University of Kansas, Lawrence, Kansas 66044

Peter M. Richards*
Department of Physics, University of Kansas, Lawrence, Kansas 66044
and Sandia Laboratories, Albuquerque, New Mexico 87115

(Received 27 November 1972)

It is shown that fruitful information can be obtained about dynamic correlations of exchange-coupled spin operators by considering both the linewidth ΔH and area A of a spin-resonance absorption curve. The product $A\,\Delta H$ is more directly related to the zero-frequency component of a dynamic correlation than is ΔH itself. The technique is applied to the linear-chain salt $Cu(NH_3)_4SO_4 \cdot H_2O$ (CTS). Measurements of A and ΔH are reported and the temperature variation of $A\,\Delta H \coth(\hbar\omega_0/2k_BT)$ is compared with the calculations of Carboni and Richards for finite chains. Below $T = 77$ K, $A\,\Delta H \coth(\hbar\omega_0/2k_BT)$ decreases as temperature is lowered. Good agreement is obtained for the applied field along the a and b axes, but results are less satisfactory along the chain c axis. The effective exchange frequency ω_e is also deduced as a function of T from A, ΔH, and Carboni and Richards's calculations of static correlation functions.

I. INTRODUCTION

The width ΔH of an exchange-narrowed electron-spin-resonance (ESR) line is related both to the static and dynamic (time-dependent) correlations of spin operators. Although many experimental studies of ΔH in strongly exchange-coupled systems have appeared in the literature, in most instances[1,2] no attempt has been made to sort out the static from the dynamic part. Since the dynamics of spin fluctuations often are of primary concern in ESR investigations, it is desirable to